Concurrent design study: Venus Atmosphere Sample Analysis mission

Girolamo Musso
girolamo.musso@tecnico.ulisboa.pt

Instituto Superior Técnico, Universidade de Lisboa, Portugal

December 2022

Abstract

Many unknowns are still present today to the most similar planet to ours in the Solar System: Venus. Although their similarities, the two planets present very different atmospheres, and it is still not clear why. Noble gases can help investigate planetary evolution theories, as they keep a trace of the planets' histories. In order to assess the feasibility of a mission to collect and analyse a sample of noble gases, a mission concept involving an aerocapture manoeuvre with in-situ analysis has been proposed and studied in the Concurrent Design Facility "Laica". This paper will cover the identification of the targets and their relative constraints, and the mission analysis. The development of an atmospheric flight propagator for the CDF will be illustrated, and a simplified design will be proposed.
Keywords: Venus atmosphere, Noble gases, Concurrent Design, Mission analysis, Trajectories

1. Introduction

Venus, Earth's evil sister, has always fascinated humans and, among them, scientists as well. However, our knowledge of the nearest and most similar planet in size and mass to ours is actually poor, and many unknowns are still present today. Indeed, although their similarities, one has oceans of liquid water and hosts a multitude of life forms, while the other is often described as a hellscape. And it is still not clear why.

A lot of uncertainties are present on planets' evolution, and space exploration has always helped the scientific community to answer many of them. Venus' exploration has however always been making engineers' life difficult, due to the harsh environment it presents but, as engineers love challenges, it became the first planet to be explored, both from orbit and from the surface.

To answer most of the questions left unanswered, samples of the atmosphere and their analysis with modern instruments are needed, justifying the focus of this work on a preliminary study of a mission to Venus' atmosphere: the Venus Atmospheric Sample Analysis mission VASA.

The mission design will be conducted in a Concurrent Design Facility (CDF); this paper will cover the identification of the targets and their relative constraints, and the mission analysis discipline.

Preliminary trade-offs have been conducted in the optic of reducing risks and complexity, leading to the choice of a direct aerocapture manoeuvre with in-situ analysis of the samples.

An interplanetary trajectory has been obtained through a theoretical method supplemented by the numerical propagation of the orbit on NASA's General Mission Analysis Tool (GMAT) [1].

In the frame of developing tools for the CDF, a Atmospheric Trajectories Propagator (ATP) has been developed during the study, and successfully validated against GMAT.

It has been then used, coupled with engineering correlations, to derive relations specific to this design to help manage the key parameters and their relations through a systemic view of the design.

Setting several arbitrary constraints some design choices have been investigated leading to the derivation of a conceptual design that would allow for an aerocapture manoeuvre able to collect the samples at the right altitude, and with good margins on the entry corridor.

2. Literature review

As in [2], the first step of a space mission analysis and design process is the definition of the objectives, to derive requirements and constraints that will help to broadly characterize the mission concept and identify drivers for each system.

Venus, the second rocky planet from the Sun, gained the epithet of Earth's 'sister planet' due to its similarity in size and mass with our planet (0.82 Earth's masses and 0.95 Earth's radius).

In spite of these analogies, the two planets

evolved in a very different way: Venus' atmosphere is dominated by CO_2 that results in a tremendous greenhouse effect, leading to an average surface temperature of 464 ℃ and a pressure of $\sim$ 93 bar.

Although many possible investigation targets exist, concerning the dynamics - namely the superrotation [3] and the relation with the Unknown Absorber [4] - and the chemistry processes - the CO_2 stabilization [5], the SO_2 inversion layer [6] and the SO_2 and H_2O abundances prediction [7], of Venus atmosphere, and the really actual debate on phosphine as possible biosignature [8], this work will focus on the planetary evolution theories and the ways to answer them.

2.1. Planetary evolution's theories

The prevailing theory upon planets' formation is the so-called solar nebula disk model: the solar system formed from a gaseous cloud where the Sun flattened the remaining gas into a disk, called "solar nebula" or "nebula disk" [9].

An initial "dry" Venus is predicted by the equilibrium condensation model, that uses plausible values of temperatures and pressures within the solar nebula to understand the chemical composition of the gas in function of the radial distance (Lewis and Prinn 1984; Kerridge and Matthews 1988, as cited in [10]).According to the model hydrous minerals were unstable where Venus formed, but stable where Earth formed, leading to a "wet" Earth; however the accretion zones for Venus and the Earth present significant overlapping zones and a real separation of their accretion zones should not be possible making the two water inventories at least similar (Weidenschilling 1976, as cited in [10]).

If the protoplanets accreted most of their final mass within the solar nebula, they would have then captured a thin H/He envelope from the disk's gases trapping as well primordial noble gases [11]. Local studies suggest that the protoplanets captured just a thin atmosphere while growing, afterwards lost while direct observations of exoplanets have shown the opposite [11].

The energy released by the decay of short-lived radiogenic isotopes, the gravitational potential and the impacts between the bodies can create magma ponds or oceans on the protoplanets [12]. While solidifying, they tend to undergo compositional fractionation, enriching the liquid phase with volatiles incompatible in the mantle minerals. Once their solubility is reached they are outgassed (Elkins-Tanton 2008; Lebrun et al. 2013; Salvador et al. 2017, as cited in [12]).

The presence of this atmosphere and its composition controls the lifetime of the magma oceans, due to the greenhouse effect that might exert on the surface. Venus' position is close to a critical value below which magma oceans could stay liquid for long enough to let the water dissociate by Sun's radiation and escape to space through hydrodynamic escape [12].

Considering this scenario, the hydrodynamic escape could remove an amount of water from Venus that could explain the observed hydrogen isotopes ratios (Donahue et al. 1997, as cited in [10]).

However, considering current Venus' hydrogen loss rate, Sun's radiation evolution in time and non-thermal hydrogen loss processes, this seems unlikely [10]. Moreover, huge amounts of O_2 should be left after losing such a big ocean, that considering current oxygen loss rates to space, should still be in the atmosphere. Removing all the O_2 through chemical reactions requires an incredible exposure of lithosphere to the atmosphere, not supported by any evidence. The possibility of an initial "moist" Venus is more plausible than a "wet" scenario [10].

The H_2O dissociation would not happen in the outer solar system due to the much smaller Sun's radiation, and it is expected that volatile-rich carbonaceous chondritic bodies travelled from the outer into the inner Solar System, hitting directly the growing terrestrial protoplanets delivering volatiles, including water, through collisions [12].

On Earth the atmospheric isotope ratios represent solar rates that are modified by a contribution from carbonaceous chondritic material although direct observations (Dixon et al. 2000; Porcelli et al. 2001; Yokochi and Marty 2004, 2006, as cited in [12]) showed how remnants of the solar nebula are still present in the mantle.

The volatiles' delivery, although considered realistic, is not well characterized in terms of delivered mass and its origins: simulations showed how the delivery of water and other volatiles should be nearly the same for Venus and Earth[13], while [14] argues that Venus might have avoided large impacts at the end of its accretion as the hypothetical Moon-forming event. Moreover, [15] reached the conclusion that the period and dimensions of the impactors play a very important role and showed how a sufficiently big impact might have even removed water from Venus.

2.2. Targets

Noble gases are of extreme importance in planetary evolution's studies as they do not react easily, keeping a trace of cataclysms such as impacts or degassing [16].

However, this ability creates a problem in terms of their identification, because of the very weak coupling to electromagnetic radiation, therefore not providing them of a strong spectral feature making it impossible to detect them through remote sens-

ing: only in-situ sampling can measure their abundances [16].

More specifically, the interest of the scientists fell over the Xenon and its isotopes, never measured precisely on Venus. They might help to understand the various volatiles-related mechanisms as: trapping of solar nebula noble gases, degassing, hydrodynamic escape, impact erosion, delivery from comets or icy planetesimals, etc. [16].

More precise Krypton and Neon isotopic ratios' measurements might help as well to discriminate between the theories upon early evolutions [16].

The homopause levels are set to 113 km for the day side and 101 km for the night side computed through the method in [17].

For completeness, the possible habitable zone altitude range is set between 48 and 62 km optimistically, and between 51 and 54 km more realistically, to solve the phosphine debate. Another possible target is the zone between the upper layer and 4 km below for chemistry processes and composition.

Table 1: Targets and altitudes.

Target	Altitude (km)
Noble gases (day)	$<$113 [17]
Noble gases (night)	$<$101 [17]
Chemistry process	66-70 [4],[5],[7]
Habitable zone (wide)	51-62 [8]
Habitable zone (precise)	51-54 [8]

2.3. Mission concept

The identified concepts were: an entry capsule, a floating balloon and an atmospheric passage. For all these concepts, the possibility of an Earth return or an in-situ analysis has been analysed.

After many trade-offs, the choice of an aerocapture manoeuvre with in-situ analysis has been proposed to collect and analyse noble gases.

A possible payload configuration for the in-situ analysis is proposed in [17]: an inlet capillary tube collects the sample, getter pumps clean it and a miniaturized Quadruple Ion Trap Mass Spectrometer (QITMS) analyses it, granting the required precision and resolution. A more detailed list of the required precisions can be found in [18].

The problematic of a hypersonic sampling is faced in the works of [19]: the author used the Direct Simulation Monte Carlo (DSMC) method to simulate numerically the transport of the various species during a Venus atmospheric passage.

Using an ablative Thermal Protection System (TPS) without traces of noble gases will avoid alteration of the noble gas ratios; the dilution of the sample however should be taken into account.

The selected concept is therefore to perform an aerocapture manoeuvre directly from the interplanetary trajectory with a periapsis lower than the homopause level, to collect a sample of noble gases to be analysed through a QITMS while orbiting the planet. It is assumed that the hypersonic sampling and the contribution of the ablated material can be quantified to dimension the payload with margins.

3. Methodology

The mission has been studied in a CDF, where concurrent engineering methods have been applied. According to [20], five key elements are needed for the concurrent design approach:

- An iterative process, started with the identification of the targets and relative constraints.
- a multidisciplinary team, in this case made by five people and two team leaders.
- An integrated design model, based on key parameters exchanged between the specialists.
- A facility, provided by the Institute for Plasmas and Nuclear Fusion (IPFN), the "Laica" CDF.
- A software infrastructure, with tools to generate and update the model (COMET) and tools for the specialists, as the one detailed in this paper.

3.1. Interplanetary trajectory

Through the ephemerides of the planets (taken from the Horizon system of the Jet Propulsion Lab (JPL) [21]) Hohmann's transfer theory has been applied, providing several launch windows and the respective arrival dates.

Different departure and arrival dates have been investigated around the theoretical values, solving the Lambert's problem for the real Δ_V with elliptic, non-coplanar orbits, thus finding optimal launch windows.

The patched conic approximation has been used with these outputs to account for Earth's gravity and find more realistic departure conditions and needed impulse.

These values have been used in GMAT to propagate the transfer accounting for precise ephemerides, external bodies perturbations, gravity models etc., allowing to find an escape velocity compatible with the launcher's limitation.

3.2. Runge-Kutta propagator

An atmospheric flight propagator has been developed as a tool for the CDF using Runge-Kutta methods.

Given the time step h and the value of the dependent variable at the present time X_n, one can compute the increment of such variable in the time step as [22]:

$$X_{n+1} = X_n + h\sum_{i=1}^{Ord} c_i k_i \quad (1)$$

Where k_i are the evaluations of the dependent variable at certain fractions of the time step. The values of k_i can be determined as [22]:

$$k_i = F(t_n + a_i h, X_n + \sum_{j=1}^{i-1} b_{ij} k_j) \quad (2)$$

The coefficients a, b and c depend on the selected propagator.

The propagator uses three Degrees of Freedom (DoF) thus the capsule will be modelled as a point mass where all the forces are applied.

The equation of motion in an inertial reference frame can be written as [23]:

$$\ddot{x} = \vec{a_G} + \vec{a_A} \quad (3)$$

where the term a_G is the gravitational acceleration and the term a_A is the term given by aerodynamic forces. At each step, the accelerations will give the increment in velocity and the velocity will give the increment in position.

The gravity potential, including the J2 term to account for the non-sphericity of the bodies is [24]:

$$U(P) = -\frac{GM}{r} + \frac{GJ_2MR^2}{r^3}(\frac{3}{2}sin^2\lambda - \frac{1}{2}) \quad (4)$$

where for the latitude λ one can write $sin^2\lambda = \frac{z^2}{x^2+y^2+z^2}$. Deriving it with respect to x,y, z, considering $r = \sqrt{x^2+y^2+z^2}$ the gravity acceleration can be written as:

$$\begin{bmatrix} a_x \\ a_y \\ a_z \end{bmatrix} = \frac{\mu_2}{|r|^3}\vec{r} + K \begin{cases} \frac{x(x^2+y^2-4z^2)}{(x^2+y^2+z^2)^{\frac{7}{2}}} \\ \frac{y(x^2+y^2-4z^2)}{(x^2+y^2+z^2)^{\frac{7}{2}}} \\ \frac{z(3x^2+3y^2-2z^2)}{(x^2+y^2+z^2)^{\frac{7}{2}}} \end{cases} \quad (5)$$

where μ is the gravitational parameter and K is the term $\frac{3}{2}\mu J_2 R^2$.

Regarding the Sun's and Earth's influence, considering both as external bodies, not influencing each other, the acceleration term is given by [25]:

$$R = \mu_d(\frac{1}{\Delta} - \frac{xx_d + yy_d + zz_d}{r_d^3}) \quad (6)$$

$$\begin{bmatrix} a_{x_G ex} \\ a_{y_G ex} \\ a_{z_G ex} \end{bmatrix} = -\mu_d \begin{cases} (\frac{x-x_d}{\Delta^3} + \frac{x_d}{r_d^3}) \\ (\frac{y-y_d}{\Delta^3} + \frac{y_d}{r_d^3}) \\ (\frac{z-z_d}{\Delta^3} + \frac{z_d}{r_d^3}) \end{cases} \quad (7)$$

with $[x_d, y_d, z_d]$ the position of the external body and $\Delta^2 = (x-x_d)^2 + (y-y_d)^2 + (z-z_d)^2$.

Regarding the aerodynamic term, the drag acceleration $\vec{a_D}$ can be written as:

$$\vec{a_D} = \frac{\vec{D}}{m} = \frac{1}{2}\rho\frac{SC_D}{m}|v|\vec{v} = \frac{1}{2}\rho_\infty\beta^{-1}|v|\vec{v} \quad (8)$$

where ρ_∞ is the atmospheric density, S is the reference area, C_D is the drag coefficient, $\vec{v}$ is the relative velocity and $\beta = \frac{m}{SC_D}$ is the ballistic coefficient.

The lift can be computed multiplying the drag by $\frac{C_L}{C_D}$ and rotating the vector by 90°.

The relative velocity can be computed as:

$$\vec{v} = \vec{v_{in}} - \vec{v_{rot}} = \vec{v_{in}} - \vec{\omega_{rot}} \times \vec{r} \quad (9)$$

where $\vec{\omega_{rot}}$ has the form $[0, 0, \omega_{rot}]$ in which ω_{rot} is the angular velocity of the planet.

The atmospheric density ρ_∞ is taken from Venus-GRAM [26].

The ephemerides are taken from the Horizon system [21].

The $Freespace$ tool supplements the ATP code with the computation of aerodynamic coefficients, heat fluxes, wall temperatures, etc. through Newtonian theory and panels' method [27].

Chosen the central body and the propagator settings, the code propagates an entry trajectory with arbitrary entry conditions. The ballistic coefficient can be fixed, or a shape file can be used to compute the C_D at each step. Lift and drag modulation events can be imposed at given points of the trajectory, as well as mid-term impulses. The propagation can be stopped at the exit of the atmosphere or can be extended to a given number of orbits.

Sutton-Graves [28] and Tauber correlations [29] are used to compute respectively convective and radiative heat fluxes; Kemp and Ridell theory [30] is used for free-molecular convective heat fluxes.

Trajectory parameters as periapsis, heat fluxes, heat loads, deceleration, etc. are outputted, as well as atmospheric data and Earth and Sun visibility conditions.

The code can be used as well to perform parametric studies, changing iteratively entry parameters or to perform Monte Carlo analyses. The code's algorithm is schematized in Figure 1

4. Results & discussion

4.1. Interplanetary trajectory

For this study, the ARIANE 6 launcher has been selected. The optimal launch window in the next 10 years is on the 20-05-2023 with a theoretical Δ_V of 2.4835 km/s. The pork chop chart relative to this window is reported in Figure 2.

The theoretical values have been implemented in GMAT where, through 94 iterations, a transfer orbit suitable for an aerocapture manoeuvre with an escape velocity of 2.4747 km/s has been achieved,

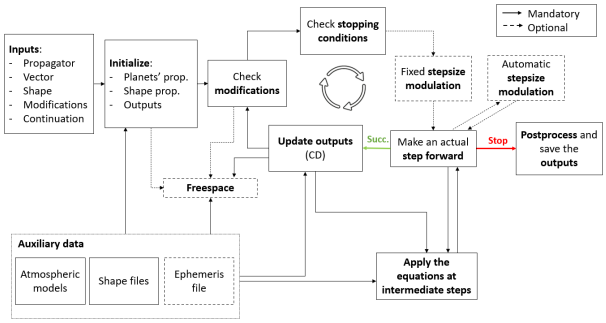

Figure 1: Algorithm workflow.

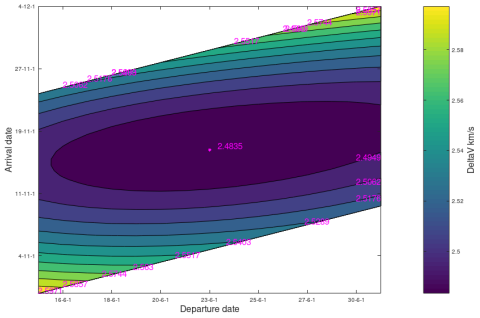

Figure 2: Launch window's pork chop chart.

iterated to achieve a day side entry. Ariane 6's limitation is 2.5 km/s [31]. The comparison between theoretical and GMAT solutions is reported in Table 2.

Table 2: Analytical and GMAT solutions' comparison.

	Analytical	GMAT	Difference
Δ_V [km/s]	2.4835	2.5438	0.0603
Julian day	30084.5	30085.0937	0.5937
i [°]	2.1809	1.4374	-0.7435
Ω [°]	180.4977	182.2398	1.7421
θ [°]	180	180	0

After $\sim$ 159 days of cruise, the arrival conditions at the edge of Venus' atmosphere reported in Table 3 are achieved.

4.2. Code validation

The atmospheric flight propagator has been validated against GMAT for an Earth's entry trajectory, as no atmospherical model was present for Venus in GMAT.

Newton's law of universal gravitation showed differences accountable to numerical precision only. The same was noticed with external gravity perturbations.

The J2 perturbation depends on the latitude: GMAT uses nutation, precession and polar motion changes of the spin axis to compute the latitude, the ATP code is instead built on an inertial reference frame, where the spin axis is fixed. The comparison has been done with a quasi-inertial reference frame updated for nutation and precession, giving errors related to the latitude computation.

Table 3: Arrival conditions.

J = 30242.8910		
Altitude [km]	Inertial v [km/s]	Path angle γ [°]
249.9939	10.8561	-9.1154
Latitude [°]	Longitude [°]	v angle [°]
-52.25	-31.19	251.83

The atmospheric model in GMAT has spatial and temporal variations of the density, therefore an ad-hoc model has been outputted for the specific trajectory. Again, small errors relative to the latitude have been found due to its presence in the computation of $v_r\vec{ot}$.

An orbit along the spin axis has been modelled through a state vector of the form $[0, 0, z, 0, 0, -v_z]$ and the comparison has been made with a fixed reference frame: the initial errors were now just numerical, however the presence of the atmospheric model resulted in a snowball effect in which numerical errors on the altitude induced bigger errors on the density and therefore on the acceleration, increasing even more the altitude errors and so on. The maximum relative errors were still on the order of 1e-5 for accelerations, velocity and position.

An adaptive step size method has been compared as well with GMAT adaptive one and, in spite of the different error control methods, the same order of magnitude was found on these errors.

4.3. Parametric study

Assuming spatial variations of the density are not relevant for Venus, the only parameters influencing the trajectories will be the entry velocity and angle, and the ballistic coefficient β.

The shape selected for this study is a 45° sphere-cone, to benefit from the heritage of Pioneer Venus multiprobe, Hayabusa, Galileo, etc. Such a shape is characterized just by the nose radius r_n and the base radius R (See Figure 3).

As scaling the shape will not affect the C_D if the flow regime does not change, defining the ratio $Ra = \frac{R}{r_n}$ one can derive a relation $C_D = f(Ra)$.

Moreover, calculating the volume as $V = f(r_n, Ra)$ and defining a capsule density $\rho_{SC} = \frac{m}{V}$ one can find relations as $\frac{\beta}{r_n}, \frac{m}{r_n^3}, \frac{m}{\beta^3} = f(Ra, \rho_{SC})$ that can help to understand which parameters one should choose according to the desired design.

Assuming a TPS of constant thickness t and a material of density ρ_{TPS}, one can compute its mass fraction over the total mass as $MF = f(Ra, \frac{t}{r_n}, \frac{\rho_{SC}}{\rho_{TPS}})$, that can be inverted and combined to the previous ones to obtain relations as $\frac{t}{r_n}, \frac{t}{\beta}, \frac{t}{m^{\frac{1}{3}}} = f(Ra, \frac{\rho_{SC}}{\rho_{TPS}, MF})$.

Although all these functions had inverse trends that did not allow obtaining an optimal design point, the function $\frac{t}{m^{\frac{1}{3}}}$ presented an optimal Ra to maximize the allowable thickness with the same mass and mass fraction, in function of the ratio $\frac{\rho_{SC}}{\rho_{TPS}}$.

Correlations between the heat load and the TPS t exist for different materials, however the heat loads HL are computed through the integral of the heat fluxes along the trajectory and cannot therefore be predicted generically: assuming Sutton-Graves formula can be used in both free-molecular and continuum regimes, one can write:

$$HL = \int_{t_0}^{t_{ex}} k_1 V(t)^3 \rho(t)^{0.5} r_n^{-0.5}\, dt + \int_{t_0}^{t_{V<V_x}} k_2 V(t)^{18} \rho(t)^{1.2} r_n^{0.49}\, dt + \int_{t_{V<V_x}}^{t_{ex}} k_3 V(t)^{7.9} \rho(t)^{1.2} r_n^{0.49}\, dt \quad (10)$$

where for Venus k_1 is 1.896e-7, k_2 is 8.497e-66 and k_3 is 2.195e-25 (to have the HL in kJ/m^2) and V_x is 10.028 km/s [28] [29].

Higher Ra will result, for the same β, in smaller r_n but lower t for the same MF, however to achieve such β a smaller mass will be needed: an optimum cannot be found as all the parameters influence each other and a direct correlation between r_n and HL cannot be achieved as the integrals in its computation depend on the specific trajectory.

The trajectory calculation depends only on the entry conditions and β and can therefore be made without such correlations, that can be used in a post-processing phase.

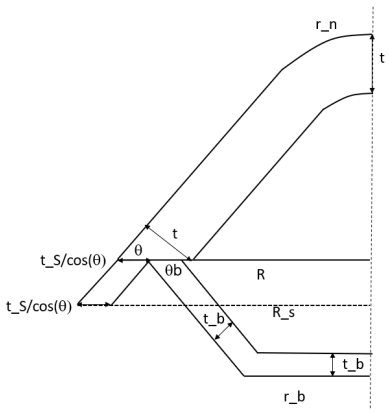

Figure 3: 45° Sphere-cone geometry.

4.4. Parametric simulations

To outline a frame of validity of the simulations, several constraints have been imposed on the solutions, some for the selected mission concept, and some related to arbitrary design choices. The following trajectories have been discarded:

- Entry trajectories, as only aerocapture manoeuvres are wanted.
- Periapsis $H > H_{max}$, due to scientific requirements.
- $\Delta_V < \Delta_{Vmin}$, to be captured after aerocapture.
- Peak heat flux $\dot{q} > \dot{q_{max}}$ for TPS material limitations.
- Heat loads $HL > HL_{max}$ for TPS limitations.
- Peak deceleration $acc > acc_{max}$ for structural limitations.

The value of H_{max} has been set to 107 km, as average between day and night homopause level, being the obtained trajectory near the terminator.

Δ_{Vmin} has been imposed to 0.8 km/s, obtained on GMAT simulating a burn at the periapsis to obtain an orbit around the planet.

$\dot{q_{max}}$ has been set to 12000 kW/m^2 to allow for the use of PICA, an ablative material suitable for after-bodies of ρ_{TPS} 274 kg/m^3 [32].

The heat load will be a function of the selected maximum MF and will be related to the used Ra and ρ_{SC}, and will vary for each ballistic coefficient.

From comparisons with previous missions, a MF of 5% was arbitrarily chosen for this study.

The value of acc_{max} cannot be related to the structural mass fraction, as no correlations between the structural loads and the structure thickness or weight exist. As the maximum quasi static load of the launcher is 6 g according to [31], therefore an arbitrary value of 10 g has been selected for acc_{max}.

Several simulations have been performed to find a wide entry corridor modifying the entry angle around the arrival one, and with β between 50 and 500 kg/m^2.

The simulated events include: an acceleration (deceleration) prior to entering the atmosphere, non-null lift and lift modulation events, drag modulation events or a combination of these. In Table 4 the simulations' conditions are reported: SF_{Vel} is the velocity scale factor, $\frac{\beta_2}{\beta_1}$ is the drag modulation ratio and H is the altitude at which the events are imposed. Variations of β with the regime have not been taken into account.

The results of these simulations can be summarized as follows:

- The corridor width is similar for all β; its boundaries' entry angles decrease for greater β.

Table 4: Simulations' conditions.

N. Sim.	SF_{Vel}	$\frac{C_L}{C_D}$	$H_{\Delta C_L}$	$\frac{\beta_2}{\beta_1}$	$H_{\Delta B}$	N. Sim.	SF_{Vel}	$\frac{C_L}{C_D}$	$H_{\Delta C_L}$	$\frac{\beta_2}{\beta_1}$	$H_{\Delta B}$
1	1	0	0	0	0	15	1	0.5	250	2	100
2	1.01	0	0	0	0	16	1	0 / 0.5	105	2	105
3	0.99	0	0	0	0	17	1	0 / 0.5	105	2	100
4	1	0.3	250	0	0	18	1	0 / 0.5	100	2	105
5	1	0.5	250	0	0	19	1	0 / 0.5	100	2	100
6	1	0 / 0.5	105	0	0	20	1	0.3 / 0.6	105	2	100
7	1	0.5 / 0	105	0	0	21	1	0.5 / 1	105	2	100
8	1	0 / 0.5	100	0	0	22	1	0.3 / 0.6	105	2	95
9	1	0	0	2	Per.	23	1	0.5 / 1	105	2	95
10	1	0	0	2	105	24	1	0.3 / 0.6	105	3	95
11	1	0	0	2	100	25	1	0.5 / 1	105	3	95
12	1	0	0	5	105	26	0.99	0.3 / 0.6	105	3	95
13	1	0	0	10	105	27	0.99	0.5 / 1	105	3	95
14	1	0.5	250	2	105	28	1	0.5 / 0 / 0.5	105	2	95

- An acceleration prior to entry seems advantage-less.
- A deceleration can mitigate thermal and structural loads. Fuel is required though, while an aerocapture avoids it.
- Providing lift increases the corridor width, saving falling trajectories.
- Too much lift will cause less Δ_V and therefore higher periapsis velocities, resulting in higher thermal and structural loads.
- The lift increases the periapsis altitude, thus mitigating the effects of the previous point.
- Drag modulation reduces structural loads if performed before the periapsis, but reduces the Δ_V as well.
- High drag modulation ratios reduce the Δ_V.
- Using drag modulation and lift can reduce loads, while maintaining acceptable Δ_V.
- The lift seems necessary to widen the corridor.

An example of these simulations with the relative constraints is reported for simulation 27 in Figure 4

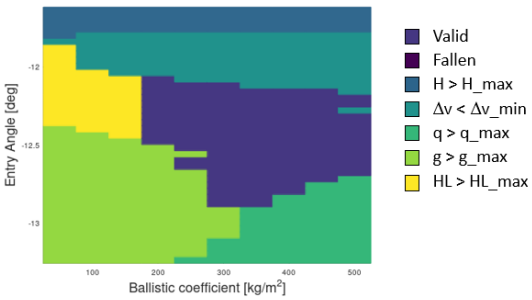

Figure 4: Example of parametric simulation.

4.5. Post-Processing

Performed the simulations, the results can be post-processed in light of what has been said before: simulations 20-27 presented the widest corridors.

However, to have drag modulation events, a "drag-skirt" could be added to decrease the ballistic coefficient, but one should dimension the capsule for the higher β, therefore, in case $\frac{\beta_2}{\beta_1}$ is 3, the range of β is now 150-1500 kg/m^2: much more difficult to achieve.

Small β produce too high decelerations at steeper angles, while too high β are difficult to achieve: the best corridors are comprised between 200 and 300 kg/m^2, however a drag modulation of 3 will result in too high masses. Using $\frac{\beta_2}{\beta_1}$ 2, the range would be comprised between 400 and 600 kg/m^2.

From the knowledge of simulations 20-23, selecting β_2 between 440 and 560 kg/m^2, lift to drag ratio between 0.3 and 0.7 and $\frac{\beta_2}{\beta_1}$ between 1.4 and 2.6, the simulations were iterated again. The $\frac{C_L}{C_D}$ has been fixed to avoid having both lift and drag modulations, and the latter has been imposed to be activated once $0.8acc_{mac}$ is reached.

The optimal corridor has been found for β 500 kg/m^2, $\frac{\beta_2}{\beta_1}$ 2.1 and $\frac{C_L}{C_D}$ of 0.6.

Using Equation 10, taking out r_n the integrals can be computed for the steepest trajectory to obtain $HL = f(r_n)$ and $t = f(r_n)$ resulting in $\frac{t}{r_n} = f(r_n)$; moreover, as the β is given one can obtain: $m = f(Ra, \rho_{SC})$, $r_n = f(Ra, \rho_{SC})$, resulting in $\frac{t}{r_n} = f(Ra, \rho_{SC})$ and therefore $MF = f(Ra, \rho_{SC})$.

Once the trajectory is computed, changing Ra and ρ_{SC} one can find the mass of the spacecraft and its nose radius, thus post-processing heat loads and heat fluxes obtaining the needed TPS thickness that can be related to the found geometry and mass to find the TPS mass fraction.

Limiting the final ρ_{SC} to 4000 kg/^{2}, the mass to 300 kg, the MF to 5% and $\dot{q_{max}}$ to 12000 kW/m^2 the results have been post-processed changing Ra and ρ_{SC} obtaining the result in Figure 5.

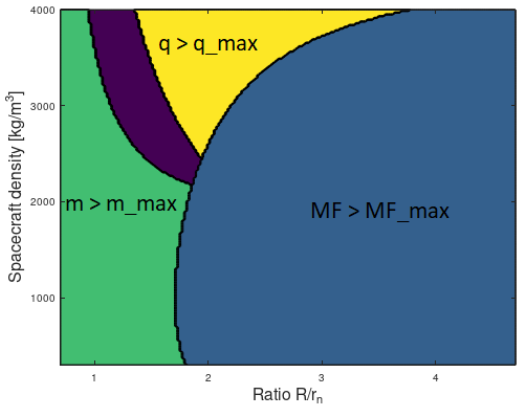

Figure 5: Constraints and range of validity.

Using Ra = 1 to benefit from Hayabusa heritage, the range of ρ_{SC} is between 3600 and 4000 kg/m^3, corresponding to masses of 300 and 243 kg.

4.6. Drag skirt and back cover

The ratio $\frac{\beta_1}{\beta_2}$ can be written as $\frac{m_2+m_S}{m_2}\frac{S_2 C_{D2}}{S_1 C_{D1}} = (1+\frac{m_S}{m_2})(\frac{R}{R_s})^2\frac{C_{D2}}{C_{D1}}$, where the subscript 1 is referred to the capsule with the skirt, and 2 without it.

The skirt will be dropped late on the trajectory, therefore will be dimensioned as an extension of the TPS; the periapsis heat load has been used to dimension it. Moreover, it will be for most of its time in free-molecular flow, therefore the free-molecular C_D has been used.

After computing the thickness of the TPS, it can be related to the outer radius R_s and to ρ_{TPS} to obtain m_S, moreover C_{D2} will be function of R_s as well, allowing to obtain R_s for the desired $\frac{\beta_1}{\beta_2}$.

To decrease ρ_{SC}, a back cover has been added to the capsule, assuming it does not influence the aerodynamic coefficients.

Of course, additional portions of the spacecraft will result in additional TPS mass, related to the dimensions of the back cover and the back cover TPS thickness.

Both spherical and conical back covers have been tried, revealing how the conical ones have smaller final MF for the same $\frac{\rho_1}{\rho_2}$, but allows for decreases in density greater than the conical ones.

It was also noticed how higher initial densities will result, for the same ρ_1, in lower mass fractions. Lastly, looking at $\frac{\rho_1}{\rho_2}$ over MF_2 one can find a maximum, where additional portions of back cover will increase too much the TPS mass without increasing enough the volume.

A conservative 10% of the stagnation peak heat flux has been assumed for this section to dimension the TPS, therefore as lighter TPS can be used for peak heat fluxes up to 1000 kW/m^2, $\dot{q_{max}}$ has been lowered to 10000 kW/m^2, pushing the yellow limit of Figure 5 to the right but allowing for a lower final mass fraction for the same $\frac{\rho_1}{\rho_2}$. Between the different materials, SIRCA was found to be the lightest for this application.

4.7. Nominal trajectory

The highest available ρ_{SC} has been therefore chosen, and the capsule was sized accordingly. The ballistic coefficient has now been updated at each step, computing the C_D through Newton's theory given the obtained shape. It has been assumed, as in [33], that C_L does not vary with the regime, therefore fixed to 0.6 of the continuum C_D.

20% uncertainty was imposed on ρ_∞ and new simulations of the corridor have been performed. A rotation of -0.47° on the interplanetary entry angle was the smallest possible for Δ_V reasons with 0.8 ρ_∞. The steepest angle, -1.05° granted a deceleration lower than acc_{max}, with 1.2ρ_∞, however the peak heat flux was now higher than 10000 kW/m^2 using 0.8ρ_∞ because the skirt was dropped too late.

A decrease of 0.08° was needed on the corridor width to achieve the imposed limit in regard to $\dot{q_{max}}$: the back cover was sized for both angles, using different materials, resulting in a mass increase of just 0.18% in case PICA is used for the back cover as well.

The final obtained dimensions are $r_n = R =$ 0.45 m, the TPS thickness is 5.5122 cm, resulting in a MF of 3.5159% over a m_2 of 300 kg. The skirt radius is $R_s =$ 0.52 m, with a TPS t_S of 4.9602 cm, resulting in a mass $m_1 =\sim$ 301 kg. Lastly, the back radius r_b is 0.063119 m, the thickness t_b will be 3.5833 cm, leading to a total mass fraction of 5.3332% and a final density of 2148 kg/m^3. The total height of the probe will be 0.6503 m. A $\frac{C_L}{C_{D_{eo}}}$ of 0.6 has been assumed. A corridor width of 0.58° has been achieved with margins.

In Table 5 some of the parameters of interest for an aerocapture manoeuvre are reported for the nominal central entry angle of -0.76°, and for the corridor extremes, including the uncertainties on the density. A visual representation is also reported in Figure 6

5. Conclusions

In the frame of developing a phase 0 conceptual study for a Venus atmospheric sample analysis, a literature survey was necessary to identify the possible targets and their location, leading to the definition of a mission concept.

As this study was conducted in a CDF, the concepts and ideas of the concurrent design have been applied, and a useful tool has been developed to be used in this context.

An interplanetary trajectory suitable for the mission concept has been derived, and its outputs have been used as starting point for the atmo-

Table 5: Trajectory characteristics.

Rotation angle [°](ρ SF)	-0.76 (1)	-0.76 (0.8)	-0.76 (1.2)	-0.47 (0.8)	-1.05 (1.2)	-1.05 (0.8)
Periapsis [km]	93.6379	93.0508	94.1238	96.6837	91.7532	90.5174
Δ_V [km/s]	1.6594	1.5971	1.7113	0.8176	2.3230	2.2334
Peak $\dot{q}$ [kW/m^2]	7319.5908	8185.0111	6725.2651	5285.4638	8606.0750	10715.3267
Total heat load [MJ/m^2]	285.5926	320.8346	258.2850	262.1825	298.8622	377.2887
Peak deceleration [g]	6.7711	6.4293	7.0223	2.5382	9.9019	9.2480
Trajectory time [s]	222	246	230	373	378	386
R_a [km]	28984.7260	31306.7610	27267.0530	291826.5133	15330.0868	16656.8091
V_a [km/s]	1.9782	1.8436	2.0913	0.2092	3.4763	3.2368
Δ_{Vap} [m/s]	22.6081	21.1991	23.6842	7.7354	37.4834	35.2942

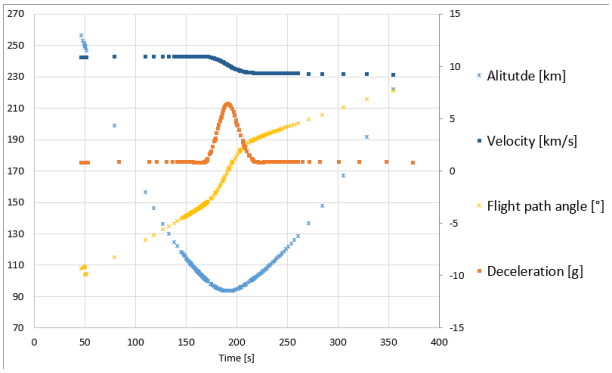

Figure 6: Aerocapture manoeuvre for entry angle -9.875° and unitary density scale factor..

spheric flight propagation.

Parametric studies have been conducted on the key parameters of the mission, identifying several aspects to be taken into account during the design.

Setting arbitrary constraints based on the nature of the mission, a conceptual design has been derived. One should however keep in mind that the presented one is just an example thought to guide the preliminary phases of a more complete design.

Indeed, a set of arbitrary constraints had been imposed, whose influence might be investigated further through more detailed studies.

Moreover, here is presented just an iteration of the whole process, that in a CDF environment will be followed by specific analyses of the heat fluxes, TPS behaviour and design, thermal control system, overall configuration and so on, leading to new requirements for instance in terms of volume or mass. A more detailed design of the same mission can be found in [34].

Nevertheless, a lot of useful knowledge has been achieved: lift has been found to be crucial to achieving a wide corridor, however, the initial design concerned just an axisymmetric probe, that can not provide much lift. Further studies should consider lift from the first phases of the design, driving the shape optimization and accounting for the related requirements and constraints.

References

[1] GMAT. User guide: http://gmat.sourceforge.net/docs/r2018a/help-letter.pdf, 2020.

[2] Wertz R. J. Larson J. W. *Space mission analysis and design*. Space technology library. Microcosm; Kluwer, El Segundo, Calif.: Dordrecht; Boston, 3rd ed edition, 1999.

[3] T. Imamura, J. Mitchell, S. Lebonnois, Y. Kaspi, A. P. Showman, and O. Korablev. Superrotation in planetary atmospheres. *Space Science Reviews*, 216(5), 2020.

[4] Y. J. Lee, A. García Muñoz, A. Yamazaki, M. Yamada, S. Watanabe, and T. Encrenaz. Investigation of uv absorbers on venus using the 283 and 365 nm phase curves obtained from akatsuki. *Geophysical Research Letters*, 48(7), 2021.

[5] Y. Marcq, C. D. Yung, and K. L. Parkinson. Atmospheric chemistry on venus: an overiview of unresolved issues. *50th Lunar and Planetary Science Conference 2019 (LPI Contrib. No. 2132)*, 313, 2019.

[6] A. C. Vandaele, O. Korablev, D. Belyaev, S. Chamberlain, D. Evdokimova, Th. Encrenaz, and L. Esposito. Sulfur dioxide in the venus atmosphere: I. vertical distribution and variability. *Icarus*, 295, 2017.

[7] P. B. Rimmer, S. Jordan, T. Constantinou, P. Woitke, O. Shorttle, R. Hobbs, and A. Paschodimas. Hydroxide salts in the clouds of venus: Their effect on the sulfur cycle and cloud droplet ph. *The Planetary Science Journal*, 2(4), 2021.

[8] J. S. Greaves, A. Richards, W. Bains, P. B. Rimmer, D. L. Clements, S. Seager, J. J. Petkowski, C. Sousa-Silva, S. Ranjan, and H. J. Fraser. Re-analysis of phosphine in venus' clouds. *arXiv preprint arXiv:2011.08176*, 2020.

[9] M. M. Woolfson. The Solar - Origin and Evolution. , 1993.

[10] B. Fegley. Atmospheric evolution on venus. 2004.

[11] J. E. Owen, I. F. Shaikhislamov, H. Lammer, L. Fossati, and M. L. Khodachenko. Hydrogen dominated atmospheres on terrestrial mass planets: Evidence, origin and evolution. *Space Science Reviews*, 216(8), 2020.

[12] H. Lammer, A. L. Zerkle, S. Gebauer, N. Tosi, L. Noack, M. Scherf, E. Pilat-Lohinger, M. Güdel, J. L. Grenfell, M. Godolt, and A. Nikolaou. Origin and evolution of the atmospheres of early venus, earth and mars. *The Astronomy and Astrophysics Review*, 26(1), 2018.

[13] M. Ya. Marov and S. I. Ipatov. Delivery of water and volatiles to the terrestrial planets and the moon. *Solar System Research*, 52(5), 2018.

[14] S. A. Jacobson, D. C. Rubie, J. Hernlund, A. Morbidelli, and M. Nakajima. Formation, stratification, and mixing of the cores of earth and venus. *Earth and Planetary Science Letters*, 474, 2017.

[15] C. Gillmann, G. J. Golabek, and P. J. Tackley. Effect of a single large impact on the coupled atmosphere-interior evolution of venus. *Icarus*, 268, 2016.

[16] K. H. Baines, S. K. Atreya, M. A. Bullock, D. H. Grinspoon, P. Mahaffy, C. T. Russell, G. Schubert, and K. Zahnle. *The Atmospheres of the Terrestrial Planets: Clues to the Origins and Early Evolution of Venus, Earth, and Mars*. University of Arizona Press, 2013.

[17] D. Nikolić, S. M. Madzunkov, and M. R. Darrach. Response of qit-ms to noble gas isotopic ratios in a simulated venus flyby. *Atmosphere*, 10(5), 2019.

[18] E. Chassefière, R. Wieler, B. Marty, and F. Leblanc. The evolution of venus: Present state of knowledge and future exploration. *Planetary and Space Science*, 63–64, 2012.

[19] J. Rabinovitch, A. Borner, M. A. Gallis, and C. Sotin. Hypervelocity noble gas sampling in the upper atmosphere of venus. In *AIAA Aviation 2019 Forum*. American Institute of Aeronautics and Astronautics, 2019.

[20] M. Bandecchi, B. Melton, and F. Ongaro. Concurrent engineering applied to space mission assessment and design. *concurrent engineering*, 2004.

[21] Horizon Ephemeris System. https://ssd.jpl.nasa.gov/horizons/app.html, 2022.

[22] G. James, D. Burley, D. Clements, P. Dyke, and J. Searl. *Modern engineering mathematics*. Pearson Education, 2008.

[23] Howard D. Curtis. *Orbital mechanics for engineering students*. Elsevier Aerospace engineering series. Elsevier Butterworth Heinemann, 1. ed., reprinted edition, 2008.

[24] R. Van Der Hilst. Essentials of geophysics. https://ocw.mit.edu/courses/12-201-essentials-of-geophysics-fall-2004/resources/ch2/, 2004.

[25] G. E. Cook. Luni-solar perturbations of the orbit of an earth satellite. *Geophysical Journal of the Royal Astronomical Society*, 6(3), 1962.

[26] H. L. Justh, A. M. D. Cianciolo, and J. Hoffman. Venus global reference atmospheric model (venus-gram): User guide. 2021.

[27] M. A. P. Lino da Silva. Freespace manual. http://esther.ist.utl.pt/freespace/manual.pdf, 2020.

[28] K. Sutton and R. A. Graves. A general stagnation-point convective-heating equation for arbitrary gas mixtures. 1971.

[29] M. E. Tauber, G. E. Palmer, and D. Prabhu. Stagnation point radiative heating relations for venus entry. 2012.

[30] N. H. Kemp and F. R. Riddell. “heat transfer to satellite vehicles re-entering the atmosphere. *Journal of Jet Propulsion*, 1957.

[31] R. Laiger. Ariane 6 user’s manual, issue 2 revision 0, 2021.

[32] S. Sepka and J. A. Samareh. Thermal protection system mass estimating relationships for blunt-body, earth entry spacecraft. In *45th AIAA Thermophysics Conference*, Dallas, TX, 2015. American Institute of Aeronautics and Astronautics.

[33] J. Li, D. Jiang, and J. Geng, X.and Chen. Kinetic comparative study on aerodynamic characteristics of hypersonic reentry vehicle from near-continuous flow to free molecular flow. 2021.

[34] M. Lino da Silva, L. Marraffa, G. Musso, H. Neiva da Silva, M. Azevedo Ferreira, Y. Jeyagobi, M. Pavanello, L. Lemos Alves, and B. M. Soares Gonçalves. A new concurrent design facility at tecnico lisbon. In *10th International systems concurrent engineering for space applications conference (SECESA)*, 2022.